Int. J. Therm. Sci. (1999) 38, 819–831

Pressure effects on the spectral behavior of the thermal field in non-reacting and low Damköhler reacting flows

Abdelhamid Bounif[a*], Abdelkader Aris [a], Iskender Gökalp[b]

[a] *Institut de génie mécanique, université des Sciences et de la Technologie, BP 1505, Elmnaouar, Oran, 31000, Algérie*

[b] *Laboratoire de combustion et systèmes réactifs, Centre national de la recherche scientifique, 1C, av. de la Recherche-Scientifique, 45071 Orléans cedex 2, France*

(Received 21 September 1998, accepted 15 March 1999)

Abstract — This study concerns the regime of distributed reaction zones of a well-stirred reactor. No mention has been made until now on the fields of the interaction between combustion and turbulence in this regime, where the Damköhler number is below unity. The aim of this paper is to investigate the fluctuating temperature structures inside the well stirred-reactor for various mean pressure situations. The experimental study is conducted by the technique of fine-wire thermoanemometry. In parallel, the fuel conversion rates of propane oxidation in all the experimental conditions are determined from a simulation work which takes into account a detailed kinetic model. The different relevant characteristics of the dynamic field are estimated by means of the k–ε model. The variation of the unmixedness and the time scales of the temperature field is compared for various pressures in the reacting and non-reacting cases. The discussion is conducted in terms of the ratio between the time scales of the scalar and dynamic fields. The main conclusions are as follows. When the reacting and non-reacting temperature fields are compared at the same mean pressure, the effect of the chemical reactions appears to be the feeding of more energy into the small scale turbulence structures. It is important to notice that the systematic decrease of time and length scales with the mean pressure in the reactor, together with a very significant increase of the dissipation rate of the temperature fluctuations, gives evidence for a positive effect of the increase of the pressure on the micromixing. © 1999 Éditions scientifiques et médicales Elsevier SAS.

turbulence modeling / temperature field / jets / pressure effects / jet-stirred reactor / thermoanemometry / reaction mechanism / low Damköhler number

Résumé — **Effets de la pression sur le comportement spectral du champ thermique en écoulement non réactifs et réactifs à faible nombre de Damköhler.** Le présent travail porte sur l'investigation du champ thermique instantané dans un réacteur auto-agité par jets gazeux. Afin d'aborder à la fois le problème du micro-mélange réalisé au sein du réacteur et celui de l'interaction combustion–turbulence à faible nombre de Damköhler, cette analyse permet de vérifier les prévisions sur les effets de compressibilité dus à la variation de la pression avec et sans réactions chimiques dans la zone des réactions distribuées. La technique expérimentale est la thermoanémométrie à fil froid. Les principales caractéristiques du champ dynamique sont estimées à partir des équations de conservation décrites par le modèle de la turbulence (k, ε). Les effets couplés de la compressibilité et de la diffusion thermique tendent à rendre les petites structures plus énergétiques et les nombres de Reynolds moyen et turbulent plus importants. Ainsi, pour des pressions croissantes, le champ thermique est, de plus en plus, constitué de petits tourbillons. Sachant que l'isotropie d'un système est conditionnée par l'existence de petites structures, on constate que l'élévation de la pression dans le réacteur favorise l'homogénéité du réacteur. En outre, le fait d'avoir pu observer l'influence de pressions supérieures à la pression atmosphérique sur le champ thermique instantané régnant dans notre configuration expérimentale constitue une tentative inédite qui mérite d'être soulignée. Connaissant en effet les besoins des motoristes en ce qui concerne la conception de codes de calcul prédictifs du fonctionnement des chambres de combustion, l'obtention de données à haute pression représente une approche nécessaire à la validation des modèles en cours d'élaboration © 1999 Éditions scientifiques et médicales Elsevier SAS.

modélisation / turbulence / champ thermique / jets / effets de la pression / réacteur auto-agité / fil froid / mécanismes réactionnels / faible nombre de Damköhler

* Correspondence and reprints.
bounif@mail.univ-usto.dz

Nomenclature

B_f	ratio of turbulence time to autoignition delay	
Da_1	Damköhler number, ratio of dynamic turbulence to chemical time scales	
Da_2	Damköhler number, ratio of thermal turbulence to chemical time scales	
$E_\theta(f)$	frequential spectrum of temperature	
f	frequency	s^{-1}
fe_θ	characteristic frequency of energetic eddies	s^{-1}
f_{lim}	limit frequency	s^{-1}
F_θ	flatness factor of the thermal probability density function	
G	production term due to buoyancy	
k	turbulent kinetic energy	$m^2 \cdot s^{-2}$
K	velocity decay rate	
L	reactor diameter	m
L_u	integral length scale of the velocity field	m
L_θ	integral length scale of the thermal field	m
le_θ	energetic length scale of the velocity field	m
p	pressure inside the reactor	Pa
P	production term due to mean strain	
Pr	Prandtl number	
R_t	ratio of thermal to dynamic turbulence time scales	
Re_t	turbulent Reynolds number	
S	density ratio ($S = \rho_a/\rho_j$)	
S_θ	Skewness factor for the probability density functions of the temperature fluctuations	
T	mean temperature inside the reactor	K
te_θ	Characteristic time for energetic thermal eddies	s
t_R	mean residence time	s
t_θ	dissipation time of temperature fluctuations	s
u_i	velocity component in the x, y and z direction in cartesian coordinate system	$m \cdot s^{-1}$
U_i	volume-weighted contravariant velocity component in ξ, η, and ζ direction	$m \cdot s^{-1}$
U_0	jet velocity at the nozzle exit	$m \cdot s^{-1}$

Greek symbols

α	thermal diffusivity	$m^2 \cdot s^{-1}$
β	expansion coefficient, $\beta = -\frac{1}{\rho}\left(\frac{\partial \rho}{\partial T}\right)_p$	K^{-1}
Γ_ϕ	general diffusion coefficient	
ε_u	dissipation rate of turbulent kinetic energy	$m^2 \cdot s^{-3}$
ε_θ	thermal dissipation rate	$K^2 \cdot s^{-1}$
η_θ	Corrsin–Obukhov length scale	m
η	Kolmogrov length scale	m
Θ^2	mean square of the temperature fluctuations	K^2
$\sqrt{\Theta^2}$	root mean square (rms) of the temperature fluctuations	K
λ_u	Taylor microscale	m
λ_θ	length microscale of temperature	m
ρ	density	$kg \cdot m^{-3}$
ν	kinematic viscosity	$m^2 \cdot s^{-1}$
μ	dynamic viscosity	$kg \cdot m^{-1} \cdot s^{-1}$
τ_c	characteristic chemical time	s
τ_{in}	autoignition delay	s
τ_η	Kolmogrov time scale	s
τ_u	large eddy time scale of the velocity	s
τ_θ	integral time scale of the thermal field	s
τ_{ij}	shear stress tensors	
Φ	equivalence ratio	
ϕ	general variable	

1. INTRODUCTION

The instantaneous temperature field in a jet-stirred flow reactor designed for chemical kinetic studies of hydrocarbon oxidation is investigated. The objective of the study is twofold. The first objective is to determine the variation of the micromixing degree of the reactive system for a wide range of pressures. The second objective is to conduct a well controlled study on the interactions between chemistry and turbulence in the distributed reaction zone produced by the jet-stirred flow reactor. This is achieved by comparing the instantaneous temperature fields in reacting and non-reacting situations and with various degrees of the reactivity of the system. The major feature of this investigation is that it corresponds to the validity domain of the dynamically passive reactive system, where the flow and thermodynamic parameters are kept unchanged between the non-reacting and reacting cases.

Figure 1 is a plot of a classical diagram for premixed turbulent combustion. The different combustion regimes are shown in this plot as a function of the turbulent flow-to-flame length scale and velocity scale ratio [1]. We believe that the regime of distributed reaction zones, where the Damköhler number is below unity, which has not been investigated until this study, is most suitable for the study of interactions between chemistry and turbulence, both experimentally and theoretically, for several reasons:

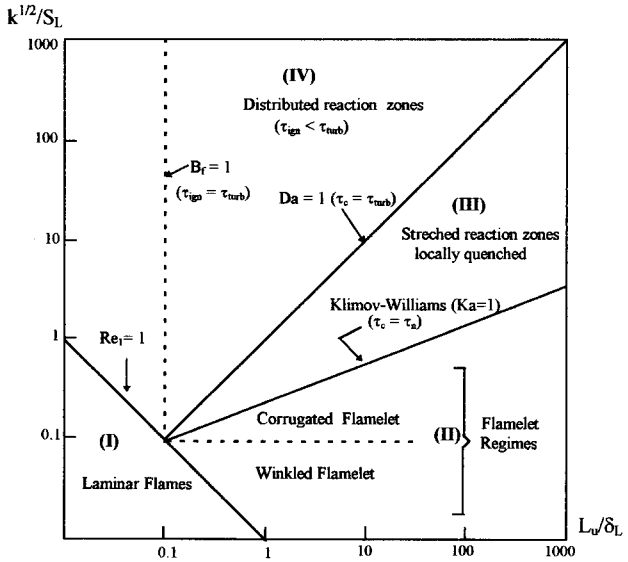

Figure 1. Premixed turbulent combustion diagram.

First, in this regime, the chemical time scale is longer than the turbulent scale and small scale turbulence can be produced [2]. These are the two necessary conditions to enhance the interaction; therefore, the condition: $Re_t > 1 > Da$, where Re_t is the turbulent Reynolds number and Da the Damköhler number, and $Bf > 1 > Da$, where Bf is the ratio between the dynamic turbulence time and the ignition delay time for the chemical reaction.

Also, as shown below, this regime may be achieved in a well-stirred reactor, where the turbulence structure is closest to the classical homogeneous and isotropic turbulence conditions, which greatly facilitates the theoretical handling of the interaction [3, 4].

2. EXPERIMENTAL DEVICE

The jet-stirred flow reactor presently investigated has been described in our previous studies on the oxidation of light hydrocarbons [5]. It consists of a fused silica-made sphere, 4 cm in diameter, located in a steel vessel which can be pressurized up to 10 atmospheres. It comprises four nozzles of 1 mm diameter opening in the equatorial plane of the sphere. The four turbulent jets achieve turbulent mixing and recirculation of the gases within the reactor, provided that the nozzle design conditions [6] are respected to ensure an optimal degree of circulation and an inlet jet velocity lower than the sonic limit speed. The flow is preheated by an electrical resistor before its admission into the reactor. The flow rates of the hydrocarbon and oxygen are measured and regulated by thermal mass-flow controllers. The pressure inside the reactor is kept constant in time by means of a pressure regulator on the exhaust line. A representation of the apparatus is given in *figure 2*. The fuel, diluted in nitrogen, is introduced separately through a capillary tube and premixed, at the entrance of the nozzles, with the principal flow, which is composed of oxygen and nitrogen. The reactor is surrounded by an electrical heater whose adequate adjustment, with that of the preheater, allows us to reduce the temperature gradient to a negligible level along a vertical diameter. The mean temperature in the reactor is measured by a chromel-alumel thermocouple and the sampling of the molecular species is achieved through a quartz sonic probe. The gas samples are analyzed by gas phase chromatography. Residence time distribution studies [5] have shown that the reactor is perfectly stirred for residence time varying from 0.01 to several seconds. But preheating of the gases is necessary and temperature homogeneity in the reactor was verified during each experiment by moving a thermocouple along a whole diameter. No radiation correction was necessary because the reactor wall temperature is nearly identical to that of the gases.

Owing to the high dilution of the fuel (0.15 to 0.5 percent by volume), the temperature rise due to reaction was less than 20 K and temperature gradient along a whole diameter were maintained around 10 K or less. The gases within the reactor were aspirated at low pressure through a sonic quartz probe, and stored in glass bottles. A multicolumn (Molecular Sieve, Porapack QS, Parapack R), multidetector (thermal conductivity, flame ionization) gas chromatography working with helium as carrier gas, was used to

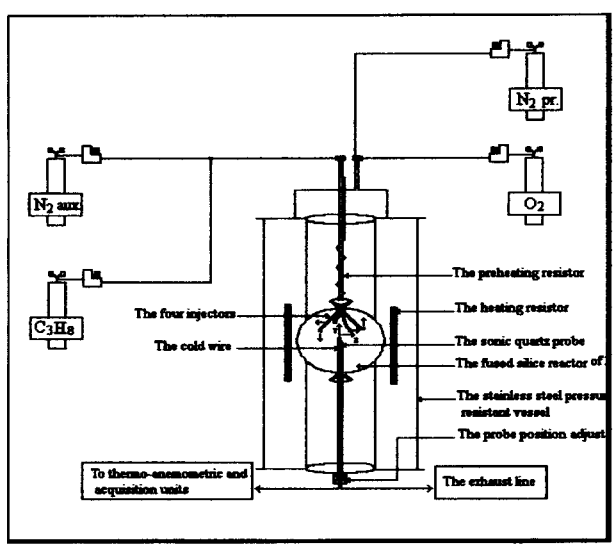

Figure 2. Schematic of experimental setup.

determine O_2, CO, CO_2, aldehydes and hydrocarbons contents of samples. The hydrogen concentration was measured on another chromatograph using nitrogen as the carrier gas, and Carle microthermistors as detector.

The temporal temperature fluctuations resulting from the turbulence is determined by a cold wire thermoanemometry along the vertical axis of the reactor. Previously calibrated in a static oven against a thermocouple, the 0.01 mm diameter platinum/rhodium sensor, supported by a probe, is introduced from the bottom of the reactor, using the probe position adjuster used for the sampling probe and the thermocouple. The fine wire is heated by a low constant current (1.5 mA), minimizing any contamination of the temperature field by the velocity fluctuations. The instantaneous temperature signal, delivered by a thermoanemometric unit (DISA55M20) and the signal conditioner, is digitized at 2 000 Hz (Nyquist frequency) and stored in a microcomputer. The thermal inertia of the wire has been numerically compensated. The acquisition has been performed via 9 blocks of 1 024 points, the resulting digitization time being much shorter than the characteristic time of turbulence, thus allowing enough points to ensure a good description of the phenomenon. Moreover, the calibration of the cold-wire has been memorized in the numerical compensation program.

3. SIGNAL PROCESSING

The digitized signal is processed to determine and compare the main characteristics of the reacting and non-reacting temperature field structures.

It is noteworthy that the signal processing through parametric methods appeared to be much more convenient for the analysis of signals observed during a short time than the Fourier transform spectral techniques. In parametric methods, we have combined the advantages of two algorithms; the root mean squares 'sans contraintes' algorithm (MCSM) which allows a good spectral resolution and Capon's algorithm [7], which gives a satisfactory estimation of spectral amplitudes. It can be considered that the thermal fluctuations are sinusoidal, more or less attenuated. An example of the fluctuating temperature data inside the reactor is exhibited on *figure 3*. Then, it is possible to convert the signal into a sum of terms with proper characteristics. Modeling the signal in this way, it will be possible to suppress the unwanted frequencies. An especially easy subtraction will allow us to eliminate noise frequencies, such as industrial 50 Hz arising from the heating line of the device. This is not possible in using the Fourier transform techniques.

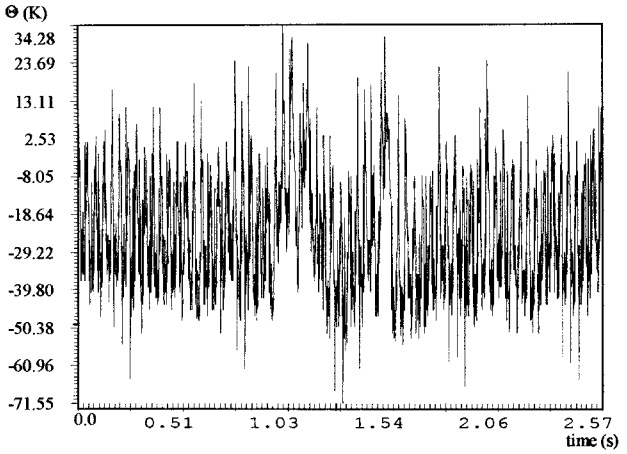

Figure 3. Fluctuating temperature signal inside the reactor under the following conditions: $p = 1$ bar, $t_R = 0.2$ s, $T = 1\,033$ K.

4. EXPERIMENTAL PROCEDURE

Each experimental run includes two phases. In the first phase, gas flows are adjusted to produce a kinetically well-known reaction for the given experimental conditions, and the instantaneous temperature measurements are performed.

In the second phase, the flow of propane is suppressed, while the flow rates of nitrogen and oxygen are kept unchanged and the instantaneous temperature measurement are repeated for this non-reacting case. As the fuel concentration is very low, the average residence times are considered as identical in both cases.

5. DYNAMIC TURBULENT FIELDS ANALYSIS

The investigation of the behavior of the temperature fluctuation in the reactor requires the estimation of the different relevant characteristics of the dynamic field. In this study, the average residence time t_R, has been adjusted large enough to ensure that the inlet jet mean velocity U_0, is lower than the speed of sound, thus allowing to neglect compressibility effects.

The dynamic field is concerned with the development of k–ε model for the numerical prediction of mixing of turbulent variable density jet. Several fundamental studies published during recent years (Thring et al. [8], Chassaing [9], Chen et al. [10], Dowling et al.[11], Pitts et al.[12], Sautet et al. [13], Panchapakesan et al. [14] and Sanders et al. [15]) have revealed complex behaviors and many underlying mechanisms which are not well understood. The main characteristics of the dynamic field are obtained by running the flow solver until

stable (in the statistical sense) values of the velocities, temperature and pressure are obtained. Extended k–ε models (also called low-Reynolds number models) which are valid in the entire domain, made of the near wall-zone (low Reynolds number) and the far-wall-zones (high Reynolds number), have been used in this study. In order to make the k–ε model asymptotically consistent in near wall turbulent flow, weighting functions are introduced [16–18] to modify the constants of Lam-Bremhorst [19].

5.1. Governing equations

The governing equations of the mean flow are obtained by Reynolds averaging the Navier-Stokes equations using a Reynolds average for the density ρ and the temperature T and a Favre average for the velocity. The Reynold stress and the turbulent heat flux are modeled using a Boussinesq hypothesis. The Navier-Stokes equations for the mean quantities are written in conservative form (Einstein convention is adopted for writing these equations on indices j and k).

5.1.1. Equation of continuity

$$\frac{\partial \rho}{\partial t} + \frac{\partial (\rho u_j)}{\partial x_j} = 0 \tag{1}$$

5.1.2. Equation of conservation of the momentum (i = 1,3)

The momentum equation, supposing that the positive direction is upwards and parallel to the gravitational field, is

$$\frac{\partial (\rho u_i)}{\partial t} + \frac{\partial (\rho u_i u_j)}{\partial x_j} = -\frac{\partial (p + \frac{2}{3}\rho k)}{\partial x_i} + \frac{\partial \tau_{ij}}{\partial x_j} + \rho g_i \tag{2}$$

when $\dfrac{\partial p}{\partial x_i} \approx \rho_a g_i$, the buoyancy term is often written as $-(\rho_a - \rho) g_i$.

5.1.3. Equation of conservation of the total energy

$$\frac{\partial (\rho e)}{\partial t} + \frac{\partial (\rho e u_j)}{\partial x_j} = -\frac{\partial (p + \frac{2}{3}\rho k) u_j}{\partial x_j} + \frac{\partial (u_j \tau_{kj})}{\partial x_j} + \frac{\partial}{\partial x_j}\left[c_p \left(\frac{\mu}{Pr} + \frac{\mu_t}{Pr_t}\right)\frac{\partial T}{\partial x_j}\right] + \frac{\partial}{\partial x_j}\left[\frac{\mu_t}{\sigma_k}\frac{\partial k}{\partial x_j}\right] \tag{3}$$

where $e = c_v T + \frac{1}{2} u_k^2 + k$, c_p and c_v are the specific heats of the mixture at constant pressure, and at constant volume.

To close the system of equation for the mean quantities, two additional transport equations may be solved for k and ε. The modeled equations can be written in a conservative form:

$$\frac{\partial (\rho k)}{\partial t} + \frac{\partial (\rho u_i k)}{\partial x_i} = \frac{\partial}{\partial x_i}\left[\left(\mu + \frac{\mu_t}{\sigma_k}\right)\frac{\partial k}{\partial x_i}\right] + G + P - \rho\varepsilon - \underline{D} \tag{4}$$

$$\frac{\partial (\rho \varepsilon)}{\partial t} + \frac{\partial (\rho u_i \varepsilon)}{\partial x_i} = \frac{\partial}{\partial x_i}\left[\left(\mu + \frac{\mu_t}{\sigma_\varepsilon}\right)\frac{\partial \varepsilon}{\partial x_i}\right] + C_1 \frac{\varepsilon}{k}(P + C_3 G) - \rho C_2 f_2 \frac{\varepsilon^2}{k} - \underline{E} \tag{5}$$

with:

$$\underline{D} = 2\mu \frac{\partial \sqrt{k}}{\partial x_i}\frac{\partial \sqrt{k}}{\partial x_i}\ ; \quad E = 2\mu \nu_t \left\{\frac{\partial^2 u_i}{\partial x_j^2}\frac{\partial^2 u_i}{\partial x_j}\right\}(1 - \delta_{ij})$$

$$G = -\beta g_i \frac{\mu_t}{Pr_t}\frac{\partial T}{\partial x_i}\ ; \quad P = \mu_t \left[\frac{\partial u_i}{\partial x_j} + \frac{\partial u_j}{\partial x_i}\right]\frac{\partial u_i}{\partial x_j}$$

$$\tau_{ij} = (\mu + \mu_t)\left[\frac{\partial u_i}{\partial x_j} + \frac{\partial u_j}{\partial x_i} - \frac{2}{3}\delta_{ij}\frac{\partial u_k}{\partial x_k}\right]\ ;$$

$$\mu_t = C_\mu f_\mu \frac{\rho k^2}{\varepsilon}\ ; \quad Re_t = \frac{k^2}{\nu \varepsilon}$$

5.2. Boundary conditions

The walls are no-slip and adiabatic boundary conditions. The boundary condition for the turbulent kinetic energy k is : $k_{y=0} = 0$.

For ε, no unique boundary condition exists and different boundary conditions have been used in a variety of applications of the k–ε model: $\left(\dfrac{\partial \varepsilon}{\partial y}\right)_{y=0} = 0$. This boundary condition is easy to implement and corresponds to an asymptotic behavior of ε in the boundary layer [20]: $\varepsilon(y) = A + B\,y + C\,y^2$, with $B \approx 0$ experimentally, $\varepsilon_{y=0} = 2\nu \left(\dfrac{\partial \sqrt{k}}{\partial y}\right)^2_{y=0}$. This last boundary condition is an approximation of the previous form, where: $\left(\dfrac{\partial \sqrt{k}}{\partial y}\right)^2_{y=0} \approx \dfrac{\sqrt{k}}{\delta}$, leading to a mean value of ε between $y = 0$ and $y = \delta$, δ denoting a small distance from the wall.

5.3. Numerical implementation

The flow transport equations can be written in a general form under the curvilinear coordinate system as:

$$\frac{1}{J}\frac{\partial}{\partial t}(\rho \phi) = \frac{\partial}{\partial \xi_i}\left(-\rho \phi U_i + \Gamma_\phi G_{ij}\frac{\partial \phi}{\partial \xi_j}\right) + \frac{S_\phi}{J} \tag{6}$$

Constants of the Boussinesq modeling and the weighting functions									
Models	C_μ	C_1	C_2	C_3	σ_k	σ_ε	Pr_t	f_μ	f_2
Lam-Bremhorst	0,09	1,44	1,92	1	1	1,33	1	1	1
Low-Reynolds	0,09	1,44	1,92	1	1	1,33	1	$\exp\left[\frac{-34}{\left(1+\frac{Re_t}{50}\right)^2}\right]$	$1-0{,}3\exp[-Re_t^2]$

where ϕ (u_i, e, k and ε) stands for a general variable to be solved, S_ϕ is the corresponding source term which includes all the terms that do not fit into this general form. Γ_ϕ is the effective diffusion coefficient associated with variable ϕ. The curvilinear coordinate is represented by ξ_i and J, U and G_{ij} are the transformation Jacobian, volume-weighted contravariant velocities and diffusion matrices respectively. Their definitions are as follows:

$$J = \frac{\partial(\xi,\eta,\zeta)}{\partial(x,y,z)} \tag{7}$$

$$U_i = \frac{u_j}{J}\frac{\partial \xi_i}{\partial x_i} \tag{8}$$

$$G_{ij} = \frac{1}{J}\frac{\partial \xi_i}{\partial x_k}\frac{\partial \xi_j}{\partial x_k} \tag{9}$$

All the partial derivatives with respect to the Cartesian coordinates occurring in equations and source terms should be evaluated in the curvilinear coordinate system by using the chain rule for partial differentiation. For the numerical computation of the governing partial differential equations, a computer code based on a finite volume code using algorithm SIMPLER for pressure linkage is employed [21]. In order to handle the complex geometry of the reactor, a boundary fitted curvilinear coordinate system and multi-block non staggered grids are used in the computation. Different numerical schemes are used to approximate the transient, convective, diffusive and source terms of the transport equations. The SIMPLER procedure is adopted to ensure mass conserved flow field solutions. The convective terms in the governing equations are approximated by a second-order central differencing scheme compensated by an adaptive artificial dissipation term to control numerical oscillation in the solution. The convective fluxes at mid-node points are evaluated by a PLDS scheme.

In order to reduce the computer memory requirements, only the orthogonal part is kept in the diffusion term, and the non-orthogonal part is lumped into the explicit part of the source terms. All the diffusion terms are discretized using second-order central differencing schemes. The equations are solved in time to steady-state solution by using an explicit four-stage time-marching scheme. The steady state is reached by continuing the computations until the differences of values of the variables between two successive time steps are insignificant.

The flow structure are computed on different meshes. The mesh spacing for the flow needs to be small enough near the wall to resolve the viscous sublayer, typically $\Delta y^+ = 0.1$, but in the center of the reactor, $\Delta y^+ = 8$ is sufficient; here the superscript ($^+$) denotes wall units ($y^+ = y\,u_t/\nu$) and ut the friction velocity at the wall.

Figures 4–6 represent the computed velocity components (u,v,w) along the longitudinal direction in the jet-stirred reactor and *figures 7–8* show the computed results of the turbulent kinetic energy, k, and its dissipation rate ε. The values of these two quantities determine the turbulence integral length and time scales, defined here as $L_u = k^{3/2}/\varepsilon$ and $\tau_{\text{turb}} = k/\varepsilon$ respectively. The turbulent Reynolds number, Re_t, defined by $k^{1/2}L_u/\nu$, had values between 180 and 600, from which the Kolmogorov length scale, $\eta_K = L_u\,Re_t^{-3/4}$, could be estimated.

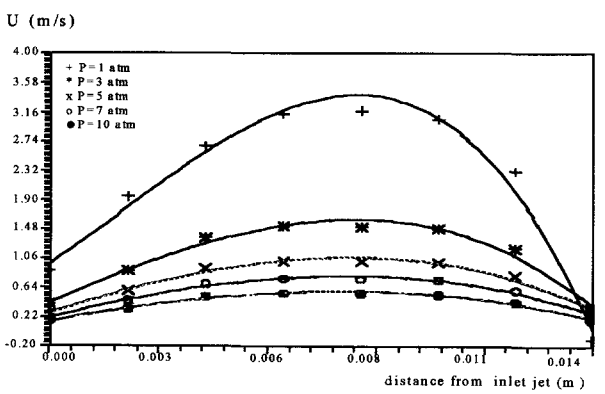

Figure 4. Computed profiles of the mean radial velocity at $p = 1$, 3, 5, 7, 10 bar, $T = 1\,030$ K, $t_s = 0.2$ s.

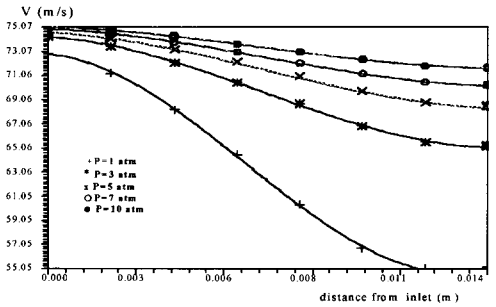

Figure 5. Computed profiles of the mean axial velocity at $p = 1, 3, 5, 7, 10$ bar, $T = 1\,030$ K, $t_s = 0.2$ s.

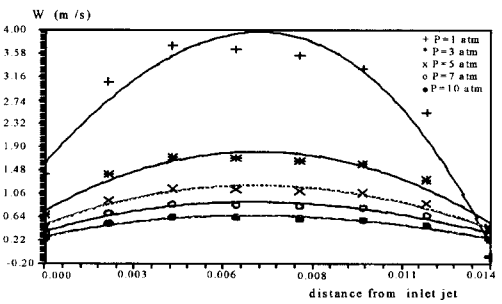

Figure 6. Computed profiles of the mean tangential velocity at $p = 1, 3, 5, 7, 10$ bar, $T = 1\,030$ K, $t_s = 0.2$ s.

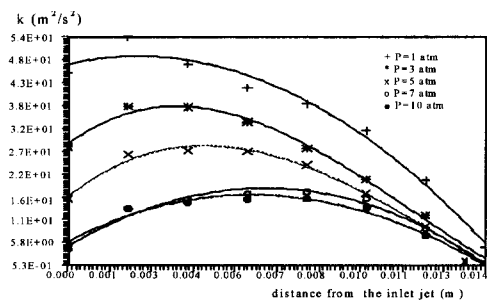

Figure 7. Computed axial evolution of the kinetic turbulent energy k at $p = 1, 3, 5, 7, 10$ bar, $T = 1\,030$ K, $t_s = 0.2$ s.

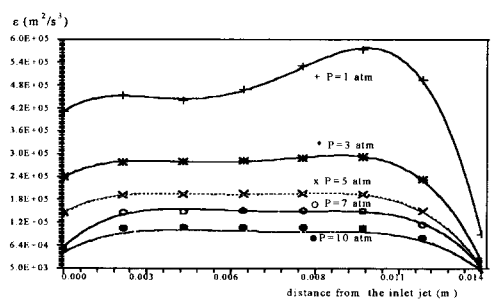

Figure 8. Computed axial evolution of the dissipation rate of the turbulent energy s at $p = 1, 3, 5, 7, 10$ bar, $T = 1\,030$ K, $t_s = 0.2$ s.

5.4 Discussion of results

Chassaing [9] and Chen [10] have shown that the axial distance before which buoyancy effects are negligible is $x_G = 0.5\, d_0\, Fr^{1/2}\, S^{1/4}$ where $Fr = \dfrac{U_0^2}{g\, d_0\, |1 - S|}$ is the Froude number and S is the initial density ratio between injected and ambient gas ($S = \rho_0/\rho_\infty \cong P_0/P_\infty$). The axial decrease of the mean velocity and turbulent parameters is influenced significantly by the mean pressure in the reactor (*figure 5*). This is directly related to the mixing of fluids of different density in the early development of the jet (near the nozzle exit). In case of a light jet ($P = 1$), the velocity will drop faster with axial distance than in a jet with $P > 1$. This is due to the conservation of the momentum flux at each cross-section of the jet. As heavy surrounding gas is mixed with the lighter jet fluid, the mean cross-section averaged density will become larger with axial distance. Consequently, the velocity must drop faster than in a jet with $P > 1$, if the momentum is to be conserved; the inverse can be argued for ($P > 1$) jets. To capture this influence of entrainment on the axial development of velocity V, the decay laws are often written using an effective diameter D_{eff} as:

$$\frac{v_j}{v_c} = K \frac{y}{D_{\text{eff}}} \quad \text{with} \quad D_{\text{eff}} = D \sqrt{\frac{\rho_0}{\rho_\infty}}$$

Using this effective diameter, one hopes to find pressure independent values for the velocity decay rate, K.

The predicted and experimental characteristics asymptotic values, K, are given as:

$S = \rho_0/\rho_\infty \cong P_0/P_\infty$	1	3	5	7	10
K	0.218	0.188	0.185	0.169	0.165
Exp. [8]	0.196	0.185	0.181	–	–
Model. [15]	0.205	–	0.201	–	0.199

The difference between the predicted and experimental results is less than 3 %, which is still considered very small, so no large influence of S on the normalized decay rates is observed. The computed values of the velocity decay rate, K, agree very well with the experiments [8, 12], and other numerical computations using a second-order Reynolds stress model (RSM) [15].

6. THE REACTION MECHANISM

We have defined the characteristic chemical time tc, from the computed concentrations profiles as the time delay for 50 % of fuel conversion. Nevertheless, for operating conditions where such a conversion rate is not

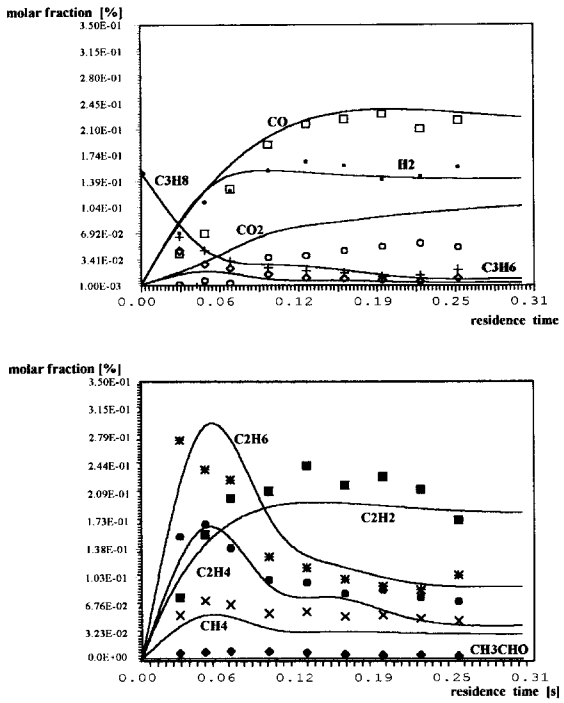

Figure 9-10. Oxidation in the jet-stirred reactor of the mixture propane, oxygen, nitrogen computed (lines) and experimental results (symbols) measured in the jet-stirred reactor (× CH_4, ■ C_2H_2, • C_2H_4, ✳ C_2H_6, □ CO, ♦ CH_3CHO, ○ CO_2, ♦ H_2, + C_3H_6, ◊ C_3H_8) under the following conditions: C_3H_8 = 0.15 %, O_2 = 0.50 %, N_2 = 98.35 %, p = 1 bar, T = 1 033 K, Φ = 1.0.

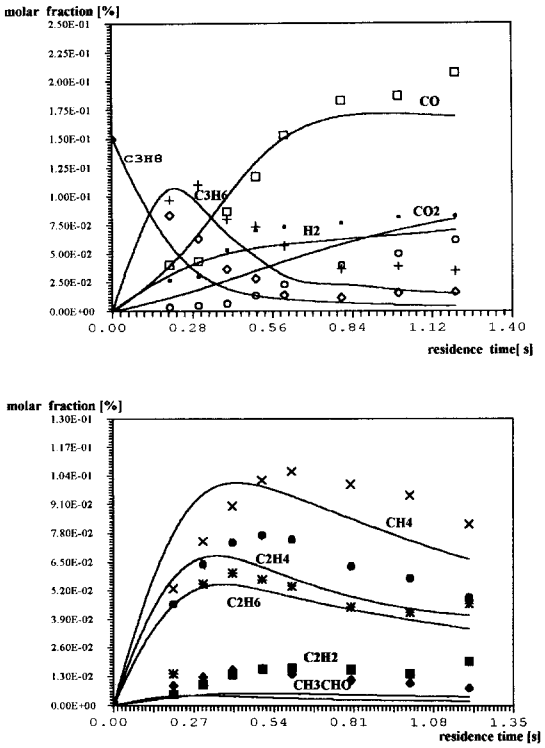

Figure 11-12. Oxidation in the jet-stirred reactor of the mixture propane, oxygen, nitrogen computed (lines) and experimental results (symbols) measured in the jet-stirred reactor (× CH_4, ■ C_2H_2, • C_2H_4, ✳ C_2H_6, □ CO, ♦ CH_3CHO, ○ CO_2, ♦ H_2, + C_3H_6, ◊ C_3H_8) under the following conditions: C_3H_8 = 0.15 %, O_2 = 0.50 %, N_2 = 98.35 %, p = 5 bar, T = 1 033 K, Φ = 1.0.

realized at a time shorter than the residence time tR, which is calculated as the reciprocal of the volume flow rate per unit volume of the reactor, it is obvious that the chemical and average residence time scales should be considered as identical.

Concentration profiles of major products (carbon monoxide, hydrogen, carbon dioxide, methane, ethylene, ethane and propane) are deduced from simulation work taking into account the detailed kinetic model. The reaction mechanism of the oxidation of the propane used in this present work has been partially published previously [22]. The complete mechanism consists of 278 reactions among 47 species. The oxidation of the propane in a JSR was computed using the computer codes (Psr–Chemkin) developed at Sandia by Kee and co-workers [23, 24]. The transport properties and thermochemical quantities form the Sandia data were also used [25]. We have used the Burcat thermochemical data [26] for the compounds not found in the chemkin data base.

Figures 9–14 represent the comparison between computed (lines) and experimental results (symbols) measured in the jet-stirred reactor [22]. No mention has been made until now on the values of the auto-ignition times and how these are affected by the turbulence. The auto-ignition time, τ_{in}, was defined as the coordinate of the maximum temperature gradient. These auto-ignition times depend only on the initial state of the mixture and the chemistry used, not on the flow, and so can used as 'reference' times with which the results of the turbulent flows examined will be compared, and thus τ_{in} can be considered as the minimum possible ignition delay time of an initially inhomogeneous mixture with initial fuel and oxidant temperatures.

The auto-ignition time in the turbulent flows is longer than the ignition delay of premixed stagnant homogeneous mixtures and this implies that heat losses due to the mixture fraction gradient associated with mixture inhomogeneities increase the induction time [27]. The delaying effect of inhomogeneities present during the residence time in turbulent mixing flows is measured by the B_f number (the ratio of the turbulence time scale to τ_{in}) and forms the discussion of this work. In the computations of the Burcat et al., the ignition delay was defined as the time at which [O] × [CO] is maximum. The ignition delay times of the propane was

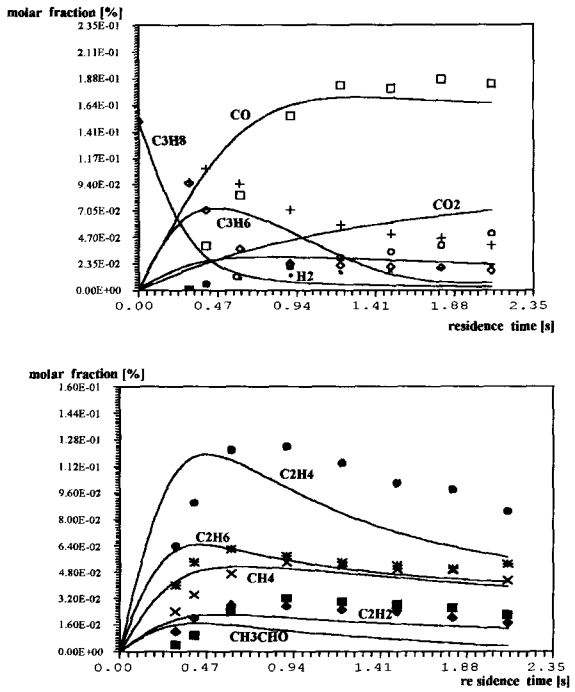

Figure 13-14. Oxidation in the jet-stirred reactor of the mixture propane, oxygen, nitrogen computed (lines) and experimental results (symbols) measured in the jet-stirred reactor ($\times$ CH_4, ■ C_2H_2, • C_2H_4, ✳ C_2H_6, □ CO, ♦ CH_3CHO, ○ CO_2, ♦ H_2, + C_3H_6, ◊ C_3H_8) under the following conditions: C_3H_8 = 0.15 %, O_2 = 0.50 %, N_2 = 98.35 %, p = 10 bar, T = 1 033 K, Φ = 1.0.

computed by (Senkin–Chemkin) codes for the pressure ranging from 1 to 10 atm. The experimental delay times measured by Burcat and al. [28] are well reproduced by the results of the computed induction times.

7. ANALYSIS OF THE INSTANTANEOUS TEMPERATURE FIELD

Gas temperature fluctuations are calculated from the simplified energy balance equation:

$$T = T_w + M_w \frac{\partial T_w}{\partial t} \tag{10}$$

where T_g and T_w are respectively the gas and wire temperatures. The anemometer time constant M_w depends on temperature, velocity and gas composition. A numerical compensation was preferred to an analog circuit, because it can take into account some of these dependencies [29]. We apply first the Nyquist interpolation formula to reconstruct the thermoanemometer signal and then the numerical compensation algorithm. The only restriction to the use of such a method is that the signal should not contain frequencies greater than half the sampling frequency. This can be guaranteed by using a high order Butterworth digital filter. This allows us to avoid the problem of errors occurring when considering high frequencies (above 1 kHz). The numerical compensation efficiency is defined as the effective fractional energy temperature spectrum restored by the numerical compensation on the energy temperature spectrum restored by an ideal compensation up to fixed frequency [30]:

$$\varphi(\omega) = \frac{1}{\omega}\int_0^{\omega} \left(\frac{1}{1+(\omega M_w)^2}\right) \cdot \left(1+(\omega M_w)^2 \left(\frac{\sin \omega T_e}{\omega T_e}\right)^2\right) \mathrm{d}\omega \tag{11}$$

where T_e is the sampling period and ω the pulsation ($\omega = 2\pi f$)

The use of central difference derivative scheme to calculate the temporal derivative, $\frac{\partial T_w}{\partial t}$ increases the efficiency of the numerical compensation up to 98 % (below 1 kHz).

The instantaneous temperature signal has been processed numerically to obtain the probability density functions and its various moments. Spectral analysis is applied to deduce the frequency spectrum of the temperature fluctuations and the relevant times scales.

From the plateau value at low frequencies of the normalized spectrum [31], $E_\Theta(f)/\Theta^2$, where f is the frequency and Θ^2 is the mean square of the temperature fluctuations, deduced as:

$$\Theta^2 = \int_0^{+\infty} E_\Theta(f)\,\mathrm{d}f \tag{12}$$

the integral time scale t_Θ of the thermal structures is obtained as follows:

$$E_\Theta(0) = 4\,\tau_\Theta\,\Theta^2 \tag{13}$$

The assumption of homogeneous and isotropic turbulence also allows the determination of the dissipation rate of the temperature fluctuations [31], ε_Θ, as:

$$\varepsilon_\Theta = 6\,\alpha \left(\frac{2\pi}{U_x}\right)^2 \int_0^{f_{lim}} f^2\,E_\Theta(f)\,\mathrm{d}f \tag{14}$$

where f_{lim} is the maximum frequency for which the spectrum is still significant, due to the limitation of the measurement line [32]. This uncertainty, Err, is expressed in term of the limit frequency flim and is deduced as:

$$Err = \frac{1}{\varepsilon_\theta}\int_{f_{lim}}^{+\infty} f^2\,E_\Theta(f)\,\mathrm{d}f \tag{15}$$

In order to evaluate this uncertainty, one have to use a model of the dissipation term of the spectrum, which is performed in the literature in several ways. In the present study, the Hinze model [31] is used, and is given by:

$$E_\Theta(f) = \frac{1}{17}\xi \left(\frac{2\pi}{U_x}\right)^{-\frac{14}{3}} \varepsilon_\Theta \varepsilon^{\frac{2}{3}} \alpha^{-3} f^{-\frac{17}{3}} \text{ if } f < f_{\text{Ny}} \quad (16)$$

$$E_\Theta(f) = 0 \qquad \text{if } f > f_{\text{Ny}} \quad (17)$$

where ξ is the Kolmogorov constant ($\xi \approx 1.50$).

Replacing the expression of the spectrum dissipation in the previous equation (15), and after integration, we obtain the maximum frequency f_{lim}, which is modeled with the Nyquist frequency (f_{Ny}), as:

$$f_{\text{lim}} = [f_{\text{Ny}}^{-8/3} + Err/\{\xi(9/68)(2\pi/U_x)^{-8/3}\varepsilon_u^{2/3}\alpha^{-2}\}]^{-3/8} \quad (18)$$

The influence of the value of the maximum frequency on the uncertainty is established in the previous equation. For instance, reducing error value to 1 %, gives a value of frequency of 625 Hz, whereas an error value of 5 % leads to a frequency value of 350 Hz.

The frequency weighted spectrum, $f E_\Theta(f)/\Theta^2$, is constructed to display the most energetic frequency range of the spectrum, whose characteristic scale is:

$$te_\Theta = \frac{1}{(2\pi f e_\Theta)} \quad (19)$$

According to recent computation methods on turbulent reacting flows, the dissipation rates of the thermal and dynamic fields can be correlated by means of a dimensionless factor:

$$R_t = \frac{\varepsilon_u \Theta^2}{\varepsilon_\Theta k} \quad (20)$$

which represents the ratio between the thermal and dynamic time scales.

Following the same concept as for the length of Kolmogorov, $\eta_k = (\varepsilon_u/\nu^3)^{-0.25}$, the length of Corrsin-Obbukhov will be defined as follows $\eta_\Theta = (\varepsilon_u/\alpha^3)^{-0.25}$.

8. SUMMARY AND DISCUSSION

With increasing pressure, the r.m.s value of the temperature fluctuations $\sqrt{\Theta^2}$ decreases and the structure of the turbulent temperature field becomes characterized by smaller time scales. As the density increases with pressure, the decrease of the kinematics viscosity and the thermal diffusivity may explain this trend. The pressure effect in the reacting case also follows the same trends as the non reacting cases. With increasing pressure, the r.m.s values and the time scales decrease progressively. However, due to the presence of chemical reactions, the $\sqrt{\Theta^2}$ values are higher they are in the non-reacting case, whereas the time scales are smaller.

The influence of the mean pressure on the fluctuating temperature field is given in *table I*. Spatial and temporal characteristics of the instantaneous thermal field, are regrouped in *table II* given below. One can remark that the integral temporal and spatial energy and dissipation scales become weaker when the pressure increases, and those characteristics of the dynamic field follow equally the same evolution (*table I*). Factor characteristics of probability densities of fluctuations of temperatures determined at different pressures with or without chemical reactions are regrouped respectively in *table II*. With the increase of pressure in the well-stirred reactor, the flatness and skewness factor respectively tend to these of a Gaussian distribution [2]. The influence of the pressure in the non-reacting and reacting cases, is that the temperature spectra are shifted towards higher frequencies with increasing reactor pressure. The dissipation spectra also follow the same evolution (*figures 15-16*). As shown in *table II*, the level of the temperature fluctuations is almost doubled compared to their non-reactive equivalents, but the time scales are reduced. This emphasizes a major result of the present study. When the reacting and non-reacting temperature fields are compared at the same mean pressure, the effect of the chemical reactions appears to be the feeding of more energy into the small scale turbulence structures (*figure 17*). The increase of the reactivity of the mixture due to increased reaction temperature then feeds preferentially the energy level of the small scales. However, due to the presence of chemical reactions, the rms values are higher than those of the non-reacting case, whereas the time scales are smaller. It is noteworthy to recall here that these differences between the reacting and non-reacting temperature fields can not be attributed to any experimental bias, for the mean temperature and the flow conditions responsible for characteristics of the fine-wire thermometer are the same for both cases. It is important to notice that the systematic decrease

TABLE I
Influence of the mean pressure on the dynamic field: $T = 1\,033$ K, $t_R = 0.2$ s.

p	(bar)	1	3	5	7	10
u_i	(m·s^{-1})	47.0	36.30	22.50	17.54	13.31
L_u	(mm)	0.859	0.810	0.715	0.646	0.570
ε_u	(W·kg^{-1}	455372	282059	198136	151490	110998
η	(mm)	0.0454	0.0226	0.0168	0.0140	0.0157
Re_t		187	324	418	494	591
k	J·kg^{-1}	53.52	37.37	27.20	21.25	15.90

TABLE II
Influence of the mean pressure on the fluctuating temperature field.

		Non-reacting cases					– – – $(C_3H_8)_0 = 0.5$ %, $\Phi = 1.0$ Reacting cases				
p	(bar)	1	3	5	7	10	1	3	5	7	10
$\sqrt{\Theta^2}$	(K)	21.6	17.8	14.3	11.7	9.94	35.5	31.5	27.51	25.6	23.3
τ_θ	(ms)	9.19	8.07	7.31	6.62	5.72	4.99	4.94	4.48	4.07	4.02
te_θ	(ms)	6.31	5.71	5.17	4.67	4.02	3.83	3.46	3.13	2.83	2.44
t_θ	(ms)	3.27	2.96	2.68	2.42	2.08	1.98	1.79	1.61	1.47	1.31
L_θ	(mm)	6.07	3.21	2.37	1.91	1.49	3.69	2.54	1.88	1.49	1.42
le_θ	(mm)	4.17	2.27	1.67	1.35	1.05	2.83	1.78	1.31	0.99	0.86
λ_θ		2.16	1.18	0.87	0.70	0.54	1.56	0.92	0.68	0.54	0.46
ε_θ	10^{-1} K^2·s^{-1}	1 727	1 725	1 747	1 729	1 727	8 422	7 697	7 639	7 611	6 609
$\sqrt{\Theta^2}/T$	(%)	2.00	1.70	1.38	1.13	0.96	3.43	3.00	2.66	2.47	2.25
S_θ		0.02	0.015	0.02	0.01	0.00	0.14	0.10	0.17	0.07	0.05
F_θ		5.41	4.18	3.66	3.48	3.26	5.45	4.26	3.83	3.64	3.59
I_t		0.78	0.61	0.53	0.47	0.39	0.42	0.37	0.32	0.29	0.28
τ_{in}	(μm)	–	–	–	–	–	148	121	40	34	27
τ_c	(ms)	–	–	–	–	–	200	140	90	60	30
$B_f = \tau_u/\tau_{in}$		–	–	–	–	–	0.80	0.96	3.42	4.11	5.31
$Da_1 = \tau_u/\tau_c$		–	–	–	–	–	0.006	0.008	0.013	0.02	0.04
$Da_2 = \tau_\theta/\tau_c$		–	–	–	–	–	0.059	0.074	0.085	0.095	0.11

of time and length scales with the mean pressure in the reactor, together with a very significant increase of the dissipation rate of the temperature fluctuations (*table II*), give evidence for a positive effect of the increase of the pressure on the micromixing. This should help to assess the usefulness of the present well stirred reactor configuration for the future high pressure chemical kinetics studies.

The variation of the parameter R_t (ratio of thermal to dynamic turbulence time scales), previously defined, with the mean pressure in the jet-stirred reactor in the reacting and non-reacting cases, is shown in *figure 18*. This figure indicates that, for a given dynamic turbulence structure, two distinct trends are shown on this figure in reacting and non-reacting cases. R_t decreases with the increase of the mean pressure

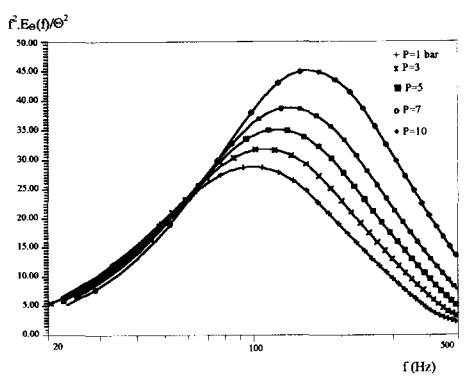

Figure 15. Dissipation spectra $f^2\,E_\Theta(f)/\Theta^2$ in the non-reacting cases under the following conditions: p = 1, 3, 5, 7, 10 bar, $t_R = 0.2$ s, $T = 1\,033$ K.

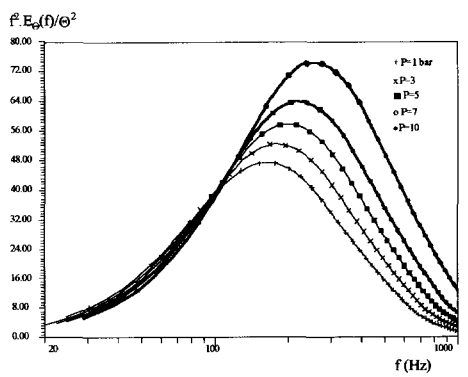

Figure 16. Dissipation spectra $f^2\,E_\Theta(f)/\Theta^2$ in the reacting cases under the following conditions: p = 1, 3, 5, 7, 10 bar, $t_R = 0.2$ s, $T = 1\,033$ K, $(C_3H_8)_0$ =0.5 %, $\Phi = 1.0$.

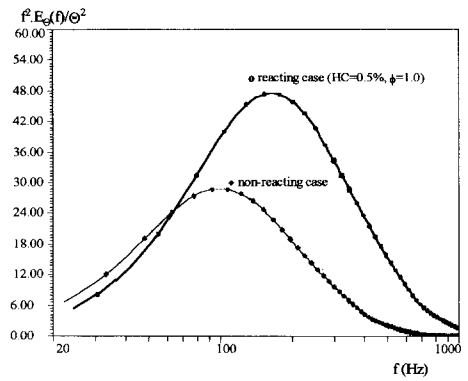

Figure 17. Dissipation spectra $f^2\,E_\Theta(f)/\Theta^2$ in the non reacting and reacting cases under the following conditions: $p = 1$ bar, $t_R = 0.2$ s, $T = 1\,033$ K in the reacting case: $(C_3H_8)_0 = 0.5$ %, $\Phi = 1.0$.

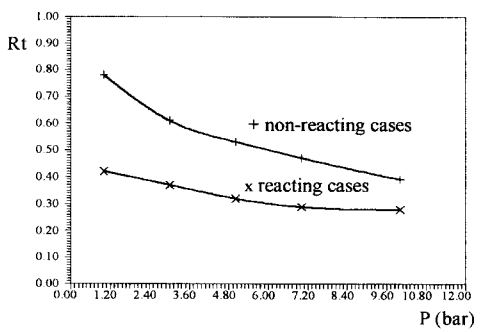

Figure 18. Variation of the ratio of thermal to dynamic turbulence time scales (R_t) with the pressure.

as in non-reacting case, albeit with stronger rate. *figure 19* shows a monotonic single trend of R_t and the temperature fluctuations intensity. I_t remains small enough, always less than 3 %, to provide satisfactory homogeneous conditions for the achievement of chemical kinetic studies. It is also important to notice that the systematic decrease of R_t and I_t with the variation of the global reactivity of the system Da and B_f numbers

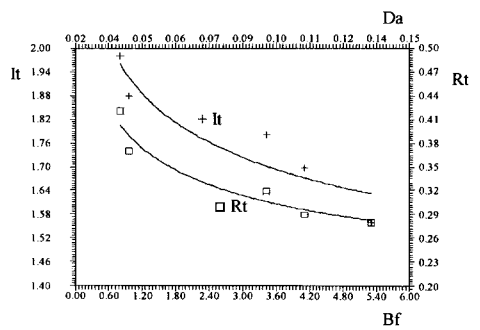

Figure 19. The variation of the ratio R_t and the intensity of thermal turbulence with B_f and Da numbers.

(*figure 19*), together with the increase of the pressure, give evidence for a positive effect of the combustion on micromixing in low Damköhler reaction zone.

REFERENCES

[1] Borghi R., On the structure and morphology of turbulent premixed flames, in: Bruno C., Ceseci C. (Eds.), Recent Advances in Aerospace Sciences, 1985, pp. 117–138.

[2] Bounif A., Gaillard F., Gökalp I., Study of interaction between turbulence and propane oxidation in a jet-stirred flow reactor, in: 20th Symp. Int. on Combustion, Orléans, poster 290, 1990.

[3] Bounif A., Gaillard F., Gökalp I., The equivalence ratio infuence on the instantaneous thermal field in low Damköhler flows, in: International Conference on Fluid and Thermal Energy Conversion '94, Univ. of Illinois at Chicago, USA, 1994, pp. 253–257.

[4] Bounif A., Gaillard F., Gökalp I., The spectral behavior of the instantaneous thermal field in a jet stirred reactor, in: Proc. Int. Conf. on Fluid and Thermal Energy Conversion '94, Univ. of Illinois at Chicago, USA, 1994, pp. 247–251.

[5] Dagaut P., Cathonnet M., Rouan J.-P., Foulatier R., Quilguars A., Boetner J.-C., Gaillard F., James H., A jet-stirred reactor for kinetic studies of homogeneous gas-phase reactions at pressure up to ten atmospheres, J. Phys. E Sci. Instrum. 19 (1986) 207–219.

[6] David R., Matras D., Règles de construction et d'extrapolation des réacteurs auto-agités par jets gazeux, Can. J. Chem. Eng. 58 (1975) 297–308.

[7] Capon J., High resolution frequency wave number spectrum analysis, P. IEEE 57 (1969) 912–926.

[8] Thring M.W, Newby M.P, Combustion length of encloded turbulent jet flames, flames and jets fuels, in: Proc. 4th Symp. on Combustion, The Combustion Institute, Pittsburgh, 1952, pp. 789–796.

[9] Chassaing P., Mélange turbulent de gaz inertes dans un jet tube libre, thèse, Toulouse, 1979.

[10] Chen C.J, Rodi W., Vertical turbulent buoyant jets, A review of experimental data, Pergamon Press, Oxford, 1980.

[11] Dowling D.R, Dimotakis P.E, First National fluid Dynamics Congress, part 2, American Institute of Aeronautics and Astronautics, 1988, pp. 982–988.

[12] Pitts W.M, Effects of global density ratio on the centerline mixing behavior of axisymmetric turbulent jets, Exp. Fluids 11 (1991) 577–612.

[13] Sautet J.-C., Stepowski D., Phys. Fluids 7 (1995) 11–19.

[14] Panchapakesan N.R., Lumley J.L., Turbulence measurements in axisymmetric jets of air and helium. Part 1. Air jet, J. Fluid Mech. 246 (1993) 197–223

[15] Sanders J.P.H., Sarh B., Gökalp I., Variabe density effects in axisymetric isothermal turbulent jets: a comparaison between a first and a second order turbulence model, Int. J. Heat Mass Tran. 40 (1997) 823–842.

[16] Launder B.E., Morse A.P., Rodi W., Spalding D.B., The prediction of free shear flows. A comparison of six turbulent models, NASA SP-311, 1972.

[17] Launder B.E., Sharma B. I., Application of the energy-dissipation model of turbulence to the calculation of the flow near a spinning disc, Lett. Heat Mass Tran. 1 (1974) 131–138

[18] Patel C., Rodi W. et Sheuerer G., Turbulence models for near-wall and low Reynolds number flows, a review, AIAAA J. 23 (1984) 1308–1319.

[19] Lam C.K.G., Bremmhorst K., A modified form of k–ε model for predicting wall turbulence, J. Fluid. Eng.–T. ASME 103 (1981) 457–460.

[20] Yudiana I., Buffat M., Implementation of a low Reynolds k–ε model for unstructured methods, in: Etma Efficient Turbulence Models for Aeronotics Brite-Euram, 1994, p. 2076–2032.

[21] Huang P.G., Leschziner M.A, in: Proc. 5th T.S.F. Symp., Cornel Univ., USA, 1985, pp. 65–80.

[22] Dagaut P., Cathonnet M., Boettner J.C., Combust. Sci. Technol. 56 (1987) 23–63.

[23] Kee R.J., Miller J.A., Jefferson J.H., Sandia National Laboratories Report SAND 80–8003, 1980.

[24] Kee R.J, Grcar J.F., Smooke M.D., Miller J.A., Sandia National Laboratories Report SAND 85-8240, 1985.

[25] Kee R.J., Dixon-Lewis G., Warnatz J., Coltrin M.E., Miller J.A., Sandia National Laboratories Report SAND 86-8246, 1986.

[26] Burcat A., Thermochemical data for combustion and calculations, in: Gardiner W.C., Jr. (Ed.). Combustion Chemistry, Springer Verlag, New York, 1984, p. 455.

[27] Bruel P., Rogg B., Bray K.N.C., On auto-ignition in laminar and turbulent non-premixed system, in: 23rd Symp. (Int.) on Combustion, 1990, pp. 759–766.

[28] Burcat A., Lifshitz A., Scheller K., Skinner G., Shock-tube investigation of ignition in propane–oxygen–argon mixtures, in: 3rd Symp. (Int.) on Combustion, 1971, pp. 745–752.

[29] Heitor M.V., Taylor A.M.K.P., Whitelaw J.H., Simultaneous velocity and tempereture measurements in premixed flame, Exp. Fluids 3 (1985) 323–335.

[30] Paranthoen P., Petit C., Lecordier J.-C., The effect of the thermal prong-wire interaction on the response of a cold wire in gaseous flows (air, argon and helium), J. Fluid. Mech. 124 (1982) 457–473.

[31] Hinze J.O., Turbulence, Mc Graw-Hill, 1959.

[32] Bounif A., Contribution à l'étude des interactions entre la turbulence et l'oxydation du propane dans un réacteur auto-agité par jets gazeux, thèse, université d'Orléans, 1990.